LA-UR-12-24411
Approved for public release; distribution is unlimited.

Title: Preliminary Interpretation of a Radionuclide and Colloid Tracer Test in a Granodiorite Shear Zone at the Grimsel Test Site, Switzerland

Author(s): Reimus, Paul W.

Intended for: Report

Preliminary Interpretation of a Radionuclide and Colloid Tracer Test in a Granodiorite Shear Zone at the Grimsel Test Site, Switzerland

Paul W. Reimus, Los Alamos National Laboartory

Introduction

In February and March 2012, a tracer test involving the injection of a radionuclide-colloid cocktail was conducted in the MI shear zone at the Grimsel Test Site, Switzerland, as part of the Colloids Formation and Migration (CFM) project. The colloids were derived from FEBEX bentonite, which is mined in Spain and is being considered as a potential waste package backfill in a Spanish nuclear waste repository. The tracer test, designated test 12-02 (second test in 2012), involved the injection of the tracer cocktail into borehole CFM 06.002i2 and extraction from the Pinkel surface packer at the main access tunnel wall approximately 6.1 m from the injection interval. The test configuration is depicted in Figure 1. This configuration has been used in several conservative tracer tests and two colloid-homologue tracer tests since 2007, and it is will be employed in an upcoming test involving the emplacement of a radionuclide-doped bentonite plug into CFM 06.002i2 to evaluate the swelling and erosion of the bentonite and the transport of bentonite colloids and radionuclides from the source to the extraction point at the tunnel wall. Interpretive analyses of several of the previous tracer tests, from 09-01 through 12-02 were provided in two previous Used Fuel Disposition Program milestone reports (Arnold et al., 2011; Kersting et al., 2012). However, only the data for the conservative tracer Amino-G Acid was previously analyzed from test 12-02 because the other tracer data from this test were not available at the time. This report documents the first attempt to quantitatively analyze the radionuclide and colloid breakthrough curves from CFM test 12-02.

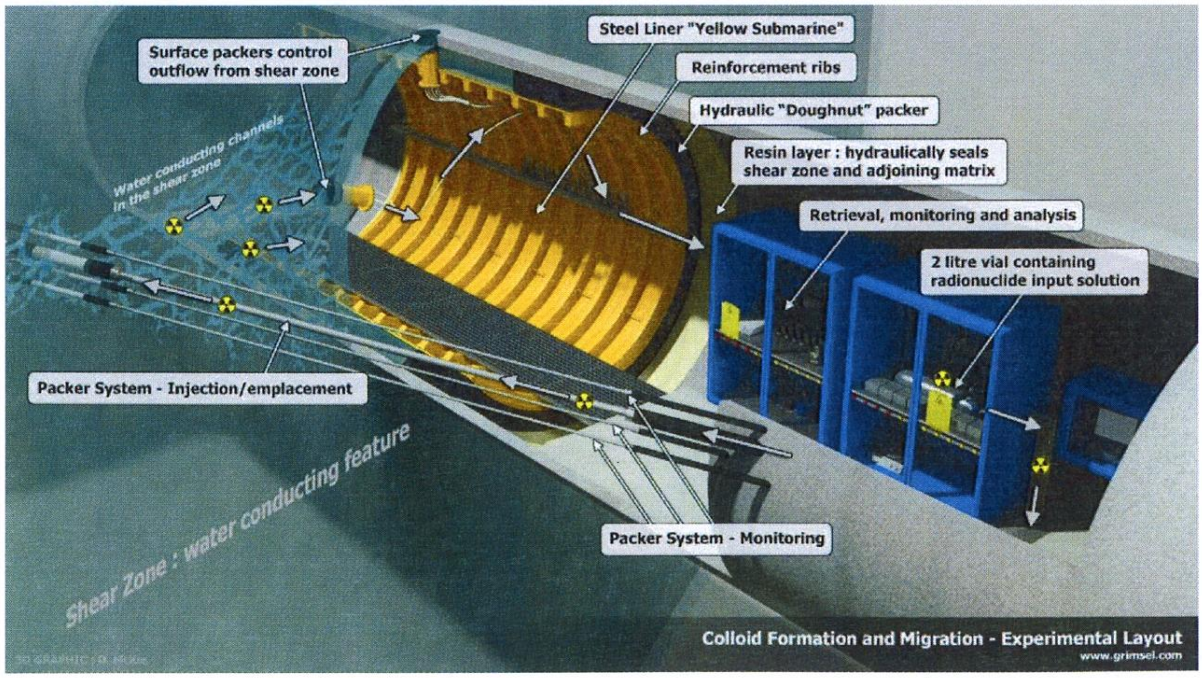

Figure 1. Schematic illustration of the CFM field testbed.

This report was originally intended to also include an experimental assessment of colloid-facilitated transport of uranium by bentonite colloids in the Grimsel system, but this assessment was not conducted because it was reported by German collaborators at the Karlsruhe Institute of Technology (KIT) that neither uranium nor neptunium adsorbed appreciably to FEBEX bentonite colloids in Grimsel groundwater (Huber et al., 2011). The Grimsel groundwater has a relatively high pH of ~9, so the lack of uranium and neptunium adsorption to clay is not surprising given the tendency for these actinides to form very stable negative or neutrally-charged uranyl- or calcium-uranyl-carbonate complexes at these pH, particularly in a water that is effectively saturated with respect to calcite. It was also observed in testing conducted at LANL earlier in 2012 that uranium did not adsorb measurably to Grimsel granodiorite in a synthetic Grimsel groundwater at pH ~8.5 (Kersting et al., 2012). Thus, the planned experimental work was not pursued because all the available information clearly pointed to an expected result that uranium transport would not be facilitated by clay colloids in the Grimsel system.

Tracer Test 12-02 Experimental Summary

Tracer test 12-02 was conducted as a weak dipole test in which the tracer cocktail was injected into the injection interval, CFM 06.002i2, at a target flow rate of approximately 0.35 ml/min while water was being continuously extracted at a rate of 25 ml/min from the Pinkel surface packer at the tunnel wall (Figure 1). The test was initiated by introducing the tracer cocktail into a flow loop that circulated through the injection interval at relatively high rate to keep the interval well mixed while maintaining a near constant net injection flow rate into the shear zone. The volume of the bottle containing the tracer cocktail was 2.25 L, and the volume of the injection flow loop was 1.0 L, so the entire injection circuit volume was 3.25 L after the tracer bottle was plumbed into the system. This arrangement resulted in an exponentially-decaying source term in the shear zone as the tracers were slowly bled out of the injection circuit.

The identity, masses, and concentrations of the tracers in the cocktail are listed in Table 1 (Schäfer, presentation to CFM working group, June 2012). Also listed in Table 1 are the reported fractions of each radionuclide that were initially partitioned to the bentonite colloids in the tracer cocktail. The tracer concentrations in Table 1 account for the dilution of the 2.25 L of cocktail into the 3.25 L total volume of the injection circuit.

The normalized concentrations of tracers (concentrations divided by injection mass) in the water extracted from the Pinkel surface packer as a function of time are shown in Figure 2. This figure also provides the normalized concentrations as a function of volume eluted in liters if the values on the x axis are multiplied by 1.5, as the extraction flow rate was 1.5 L/hr. As of the time of this writing, analytical data were not yet available for the Np or Th that were injected in the test.

All the data shown in Figure 2 should be considered preliminary, particularly the Pu and Am concentrations that were measured by ICP-MS at KIT, which were generally close to detection limits. The ^{22}Na, ^{137}Cs and ^{133}Ba concentrations were measured by gamma spectrometry at both the Paul Scherer Institute (PSI) in Switzerland and at KIT, and the data from the two institutions were found to be in excellent agreement. The Amino-G acid concentrations were measured in the field using an inline fluorimeter and were found to be in good agreement with offline

Table 1. Tracer injection masses, concentrations (in 3.25 L), and fraction partitioned to colloids in CFM Tracer Test 12-02. Radionuclide masses are calculated from activities reported by Schäfer (presentation to CFM working group, June 2012).

Tracer or Radionuclide	Injection Mass, µg	Injection Concentration, µg/L	Fraction Partitioned to Colloids
Amino G Acid (AGA)	3706	1140	0
Bentonite Colloids	228,150 ± 5600	70,200 ± 1700	N/A
^{22}Na	0.0045	0.00139	0-0.03
^{133}Ba	0.268	0.082	0.24-0.34
^{137}Cs	0.499	0.153	0.97
^{232}Th	2.0	0.616	0.95-0.97
^{237}Np	4.69	1.44	0
^{243}Am	0.038	0.118	1.0
^{242}Pu	1.267	0.39	1.0

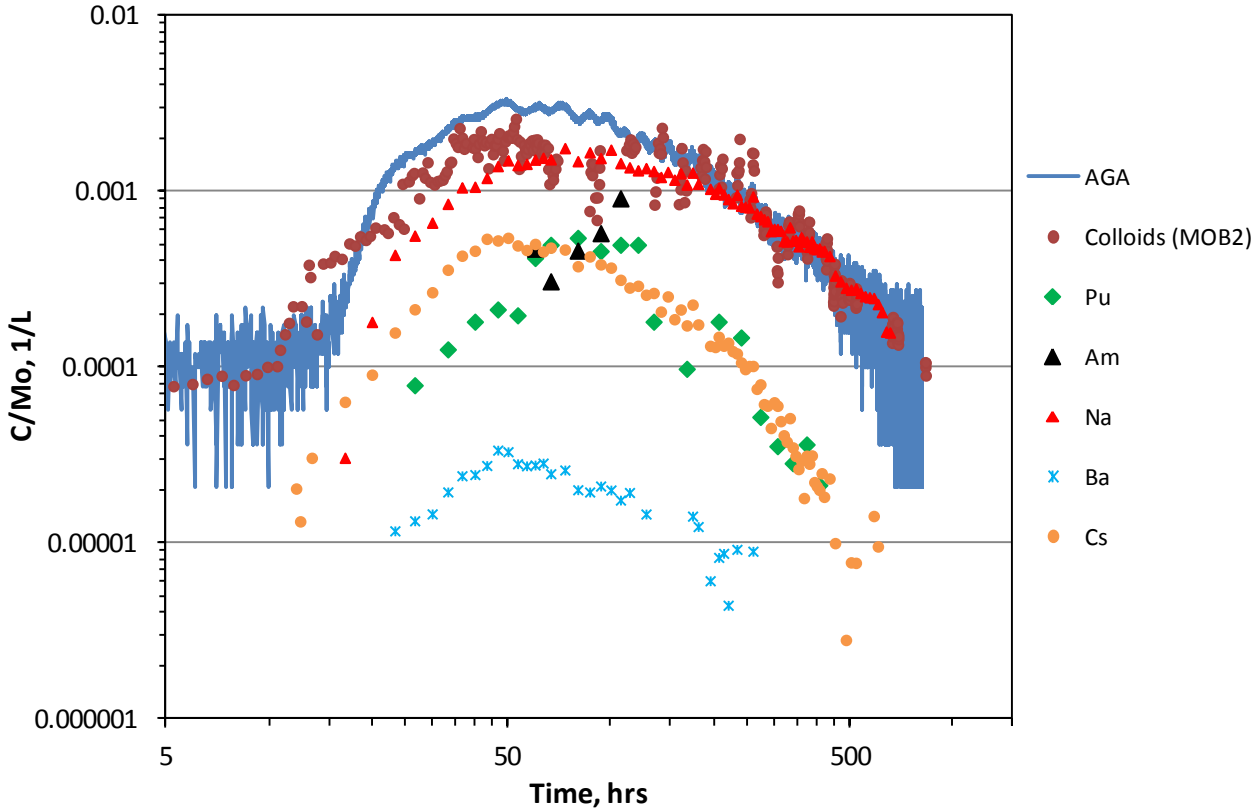

Figure 2. Normalized breakthrough curves of all tracers in CFM Tracer Test 12-02.

measurements conducted at KIT. The colloid concentrations were measured in the field using a mobile laser-induced breakdown detection (LIBD) system operated by KIT personnel. Offsite colloid measurements were also conducted by PSI using a single-particle counter (SPC), and although quantitative normalization was not possible with these data because of the lack of an

injection cocktail measurement, the general trends in the LIBD and SPC data were in good agreement (Figure 3).

Figure 4 shows the concentrations of Amino-G acid (henceforth referred to as AGA), the conservative fluorescent tracer used in the test, in the injection loop as a function of time. This tracer was the only one measured in the injection loop, using a second inline fluorimeter. The exponential decay of the Amino-G acid concentration in the injection circuit appears as a linear trend on the log-linear plot of Figure 4. It is apparent that there is a break in the slope in Figure 4 at approximately 130 hrs into the test, which can be attributed to a change in the net injection flow rate rate from the injection circuit into the shear zone. Assuming a well-mixed injection circuit, the negative of the slope of this trend line is equal to Q/V, where Q is the net injection volumetric flow rate and V is the injection circuit volume. Given the known injection circuit volume of 3.25 L, the injection rates can be deduced from the slopes of Figure 4 to be 0.46 ml/min before 130 hr and 0.36 ml/min after 130 hrs. These flow rates were used in the subsequent interpretive analyses of the tracer test.

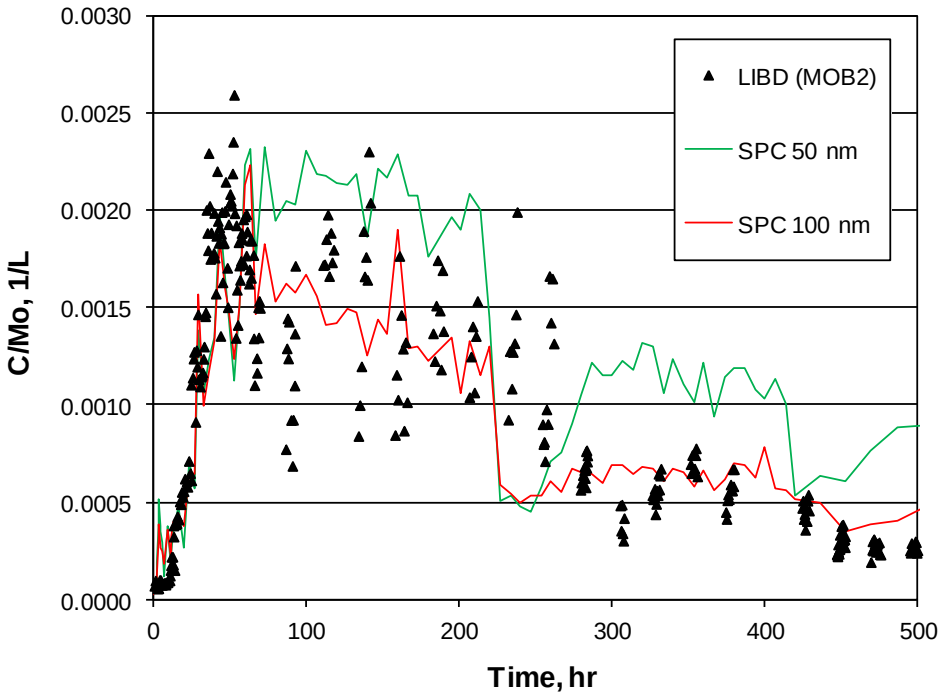

Figure 3. Comparison of colloid breakthrough curves in tracer test 12-02 from the mobile LIBD system (MOB2) operated by KIT at the Grimsel Test Site and the PSI single particle counter (50 and 100 nm channels). The SPC data are not normalized but rather are multiplied by an appropriate constant to yield approximately the same normalized concentrations as the LIBD data. SPC data are courtesy of Claude Degauldre, PSI.

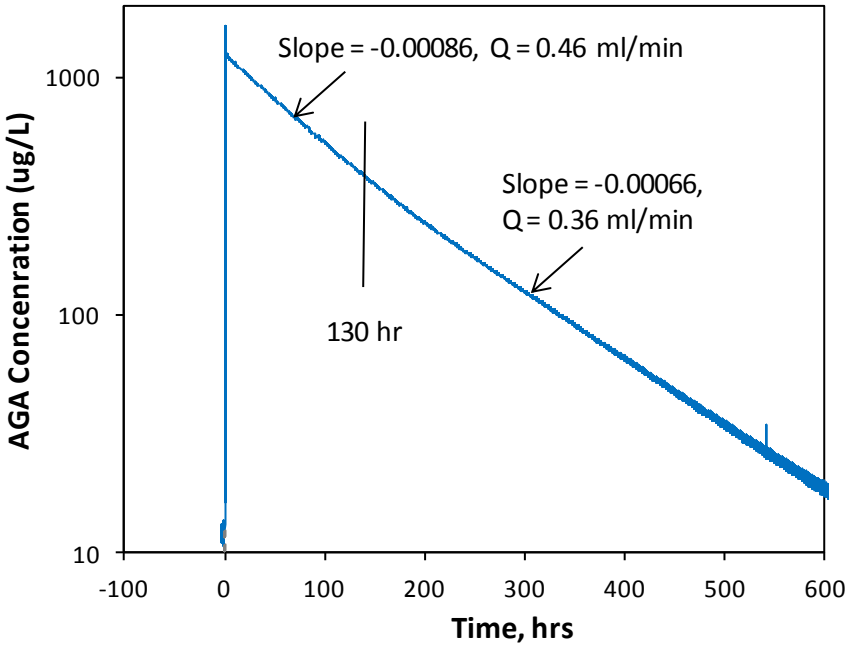

Figure 4. AGA concentration as a function of time in the injection circuit.

Interpretive Methods

The interpretation of the Amino-G acid (conservative tracer) breakthrough curve in Test 12-02 was conducted using the RELAP (REactive transport LAPlace transform) model (Reimus et al., 2003). RELAP is a semi-analytical model that uses a Fourier transform inversion method to solve the Laplace-domain transport equations in either a single- or a dual-porosity system. The model can account for a well-mixed injection function as well as diffusion between fractures and matrix and also linear, first-order reactions in both fractures and matrix. The very rapid execution of the model makes it ideal for the multiple simulations needed for parameter estimation.

RELAP was used to estimate a mean residence time, Peclet number (path length divided by dispersivity), and a tracer mass fraction participating in the test for the AGA. It was initially assumed that there was no matrix diffusion of the AGA, which is considered a reasonable assumption because of the relatively large size and hence small diffusion coefficient of this molecule and also because of the low matrix porosity of the granodiorite and the relatively short time scale of the tracer test. However, it is certainly recognized that there is potential for matrix diffusion within the altered shear zone, which has a somewhat higher porosity than the unaltered matrix.

Figure 5 shows the results of two RELAP fits to the AGA breakthrough curve over the first 360 hours of the test, which captures the majority of the tracer recovery. The two fits differ in that the net injection flow rate into the shear zone was assumed to be either 0.488 ml/min or 0.363 ml/min, respectively. RELAP is not capable of simulating changes in injection or production flow rates, so these two rates were used as end members (note that the extraction flow rate

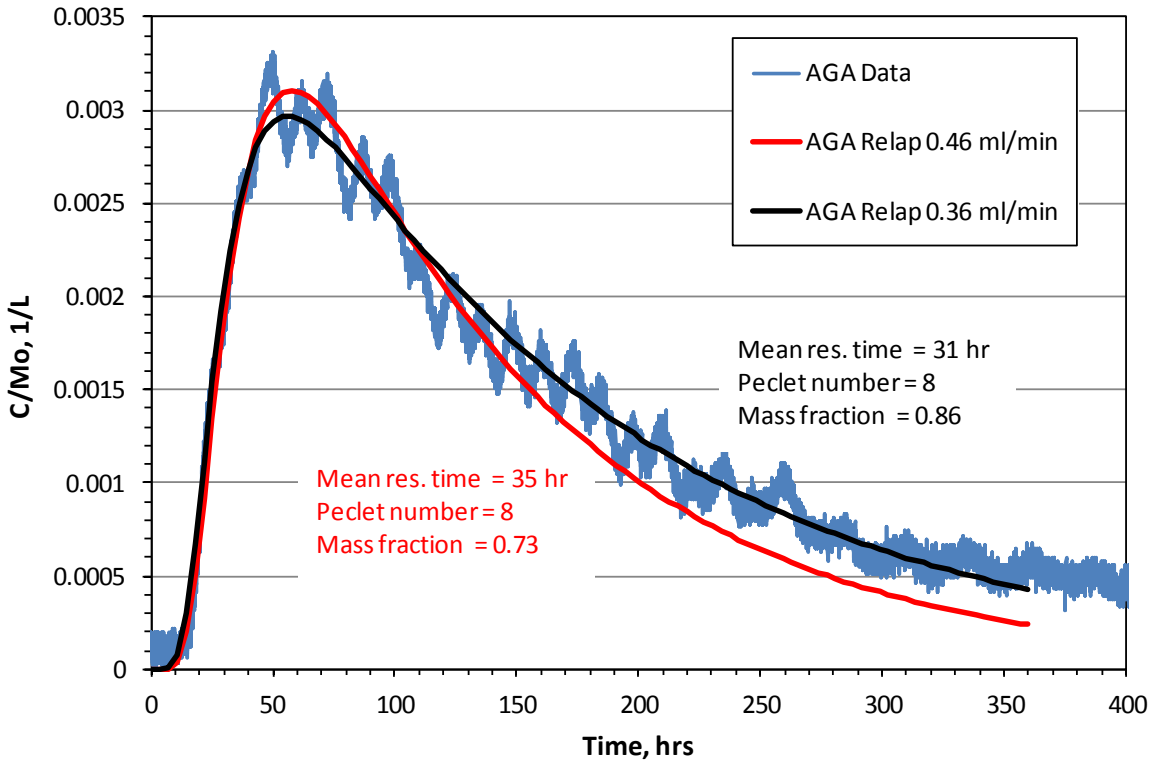

Figure 5. RELAP fits to the AGA breakthrough curve assuming either a 0.46 ml/min injection flow rate (over first 130 hrs) or a 0.36 ml/min injection rate (remainder of test).

remained essentially constant throughout the test). The mean residence time, Peclet number, and mass fraction associated with each fit are shown in Figure 5. Of interest is the difference in mass fraction between the two fits, which can be largely attributed to the differences in the effective dilution factor (ratio of extraction rate to injection rate) for the two cases. A higher mass fraction is deduced to have participated in the test when the injection flow rate is lower because a larger dilution factor is assumed. The actual AGA mass recovery over the entire ~1200 hrs of the test was calculated to be greater than 96%, which indicates that there was more mass in the tail of the breakthrough curve than either of the fits through 350 hrs would predict (it could also suggest that the sawtooth shape of the observed breakthrough curve may have contained more mass than the smoothed fit).

The physical transport parameters (mean residence time, Peclet number and mass fraction) deduced for the AGA at the higher injection flow rate of 0.46 ml/min were assumed to apply to all the other tracers for interpretive purposes. The only exception was that the Peclet number for the colloids was allowed to vary from that of the solutes because it was quite evident that the colloids exhibited a slightly earlier breakthrough than the solutes, suggesting greater dispersion of the colloids in the shear zone. Although it may seem more logical to use the parameters obtained when assuming the lower injection flow rate because this rate applied over all but the first 130 hours of the test, the first 130 hours correspond to when the first breakthrough and peak concentrations of most of the tracers occurred, and these key features have a strong influence on estimates of model transport parameters.

For analyzing the tracer breakthrough curves other than AGA, it was recognized that a more sophisticated model than RELAP was needed, particularly since it was evident that some of the solute tracer responses were likely influenced by solute-colloid interactions that RELAP cannot simulate. Also, it was desirable to explicitly account for the change in the injection flow rate that occurred 130 hrs into the test. For these reasons, a 2-D numerical model was adapted from previous work to account for all the processes that were considered potentially important to explain the tracer breakthrough curves. This model solves the following equations simultaneously:

Colloid Transport in Fractures:

$$\text{Mobile: } \frac{\partial C_{col}}{\partial t} + v_f \frac{\partial C_{col}}{\partial x} - D_c \frac{\partial^2 C_{col}}{\partial x^2} + k_{fc} C_{col} - k_{rc} S_{col} + k_{fci} C_{col} - P_{col} = 0 \quad (1)$$

$$\text{Immobile: } \frac{\partial S_{col}}{\partial t} - k_{fc} C_{col} + k_{rc} S_{col} - k_{fci} C_{col} = 0 \quad (2)$$

Solute Transport in Fractures:

$$\frac{\partial C}{\partial t} + v_f \frac{\partial C}{\partial x} - D_f \frac{\partial^2 C}{\partial x^2} + k_{1f} C C_{col} \left(1 - \frac{C_1}{C_{col} S_1^0}\right) + k_{2f} C\, C_{col} \left(1 - \frac{C_2}{C_{col} S_2^0}\right) +$$
$$\left(\frac{\rho_f}{\eta}\right) k_{fa} C \left(1 - \frac{S_a}{S_a^0}\right) + \left(\frac{\rho_f}{\eta}\right) k_{fb} C \left(1 - \frac{S_b}{S_b^0}\right) + k_{1f} C S_{col} \left(1 - \frac{C_{filt,1}}{S_{col} S_1^0}\right) + k_{2f} C S_{col} \left(1 - \frac{C_{filt,2}}{S_{col} S_2^0}\right) - \quad (3)$$
$$k_{1b} C_1 - k_{2r} C_2 - k_{1b} C_{filt,1} - k_{2r} C_{filt,2} - \left(\frac{\rho_f}{\eta}\right) k_{ra} S_a - \left(\frac{\rho_f}{\eta}\right) k_{rb} S_b - \frac{\phi D_m}{b\eta} \left.\frac{\partial C_m}{\partial y}\right|_{y=b} = 0$$

Solute Transport on mobile colloids (in fractures) while adsorbed to colloid sites 1 and 2:

$$\frac{\partial C_1}{\partial t} + v_f \frac{\partial C_1}{\partial x} - D_c \frac{\partial^2 C_1}{\partial x^2} - k_{1f} C C_{col} \left(1 - \frac{C_1}{C_{col} S_1^0}\right) - k_{rc} C_{filt,1} + \quad (4)$$
$$k_{1r} C_1 + k_{fc} C_1 - P_{col} S_a = 0$$

$$\frac{\partial C_2}{\partial t} + v_f \frac{\partial C_2}{\partial x} - D_c \frac{\partial^2 C_2}{\partial x^2} - k_{2f} C C_{col} \left(1 - \frac{C_2}{C_{col} S_2^0}\right) - k_{rc} C_{filt,2} + \quad (5)$$
$$k_{2r} C_2 + k_{fc} C_2 - P_{col} S_b = 0$$

Solute Transport in Matrix:

$$\frac{\partial C_m}{\partial t} - D_m \frac{\partial^2 C_m}{\partial y^2} + \left(\frac{\rho_b}{\phi}\right) k_{fam} C_m \left(1 - \frac{S_{am}}{S_{am}^0}\right) + \left(\frac{\rho_b}{\phi}\right) k_{fbm} C_m \left(1 - \frac{S_{bm}}{S_{bm}^0}\right) - \left(\frac{\rho_b}{\phi}\right) k_{ram} S_{am} - \left(\frac{\rho_b}{\phi}\right) k_{rbm} S_{bm} = 0 \quad (6)$$

Immobile Solute in Fractures (sorption sites a and b):

$$\frac{\partial S_a}{\partial t} - k_{fa} C \left(1 - \frac{S_a}{S_a^0}\right) + k_{ra} S_a = 0 \quad (7)$$

$$\frac{\partial S_b}{\partial t} - k_{fb} C \left(1 - \frac{S_a}{S_b^0}\right) + k_{rb} S_b = 0 \quad (8)$$

Immobile Solute in Matrix (sorption sites a_m and b_m):

$$\frac{\partial S_{am}}{\partial t} - k_{fam} C \left(1 - \frac{S_{am}}{S_{am}^0}\right) + k_{ram} S_{am} = 0 \quad (9)$$

$$\frac{\partial S_{bm}}{\partial t} - k_{fbm} C \left(1 - \frac{S_{bm}}{S_{bm}^0}\right) + k_{rbm} S_{bm} = 0 \quad (10)$$

Immobile Solute adorbed onto Immobile Colloids in Fractures (colloid sites 1 and 2):

$$\frac{\partial C_{filt,1}}{\partial t} - k_{1f} C S_{col} \left(1 - \frac{C_{filt,1}}{S_{col} S_1^0}\right) - (k_{fc} + k_{fci}) C_1 + k_{rc} C_{filt,1} + k_{1r} C_{filt,1} = 0 \quad (11)$$

$$\frac{\partial C_{filt,2}}{\partial t} - k_{2f} C S_{col} \left(1 - \frac{C_{filt,2}}{S_{col} S_2^0}\right) - (k_{fc} + k_{fci}) C_2 + k_{rc} C_{filt,2} + k_{2r} C_{filt,2} = 0 \quad (12)$$

where, C_{col} = concentration of colloids in solute phase, g/cm^3
S_{col} = colloid concentration on fracture surfaces, g/cm^3
C = solution concentration of solute in fractures, g/cm^3
C_m = solution concentration of solute in matrix, g/cm^3
S_a = sorbed concentration of solute on fracture surface site a, g/g
S_b = sorbed concentration of solute on fracture surface site b, g/g
C_1 = concentration of solute sorbed to site 1 on mobile colloids, g/cm^3
C_2 = concentration of solute sorbed to site 2 on mobile colloids, g/cm^3

$C_{filt,1}$ = concentration of solute sorbed to site 1 on immobile colloids, g/cm^3
$C_{filt,2}$ = concentration of Pu on sorbed to site 2 on immobile colloids, g/cm^3
S_{am} = sorbed concentration of solute on matrix surface site a_m, g/g
S_{bm} = sorbed concentration of solute on fracture surface site b_m, g/g
P_{col} = colloid production rate in fractures, g/cm^3-s
v_f = fluid velocity in fractures, cm/s
D_f = solute dispersion coefficient in fractures, cm^2/s
D_c = colloid dispersion coefficient in fractures, cm^2/s
D_m = solute molecular diffusion coefficient in matrix, cm^2/s
ρ_f = effective bulk density within fractures, g/cm^3
ρ_B = bulk density in matrix, g/cm^3.
η = porosity within fractures
ϕ = matrix porosity
b = fracture half aperture, cm
k_{fc} = colloid filtration rate constant (1/s) = λv_f, where λ = filtration coefficient (1/cm)
k_{rc} = reverse colloid filtration (detachment) rate constant, 1/s.
k_{fci} = irreversible colloid filtration rate constant, 1/s
k_{fa} = rate constant for sorption of solute onto fracture surface site a, ml/g-s
k_{ra} = rate constant for desorption of solute from fracture surface site a, 1/s
k_{fb} = rate constant for sorption of solute onto fracture surface site b, ml/g-s
k_{rb} = rate constant for desorption of solute from fracture surface site b, 1/s
k_{fam} = rate constant for sorption of solute onto matrix surface site a_m, ml/g-s
k_{ram} = rate constant for desorption of solute from matrix surface site a_m, 1/s
k_{fbm} = rate constant for sorption of solute onto matrix surface site b_m, ml/g-s
k_{rbm} = rate constant for desorption of solute from matrix surface site b_m, 1/s
k_{1f} = rate constant for sorption of solute onto colloid surface site 1, ml/g-s
k_{1r} = rate constant for desorption of solute from colloid surface site 1, 1/s
k_{2f} = rate constant for sorption of solute onto colloid surface site 2, ml/g-s
k_{2r} = rate constant for desorption of solute from colloid surface site 2, 1/s
S_1^0 = maximum solute capacity on colloid sorption site 1, g/g colloid
S_2^0 = maximum solute capacity on colloid sorption site 2, g/g colloid
S_a^0 = maximum solute capacity on fracture sorption site a, g/g solid
S_b^0 = maximum solute capacity on fracture sorption site b, g/g solid
S_{am}^0 = maximum solute capacity on matrix sorption site a_m, g/g solid
S_{bm}^0 = maximum solute capacity on matrix sorption site b_m, g/g solid

Figure 6 shows the system geometry and boundary conditions assumed in the model. The parallel-plate fracture domain is one node wide, implying that concentration gradients across the fracture aperture are rapidly leveled by diffusion and/or advective mixing. Solute diffusion between fractures and matrix is assumed to be perpendicular to the fracture flow direction. The matrix nodes can be specified to have variable spacing with different porosities and different solute diffusion coefficients as a function of distance away from the fracture wall. Thus, fracture coatings or gradients in porosity or diffusion coefficients can be simulated.

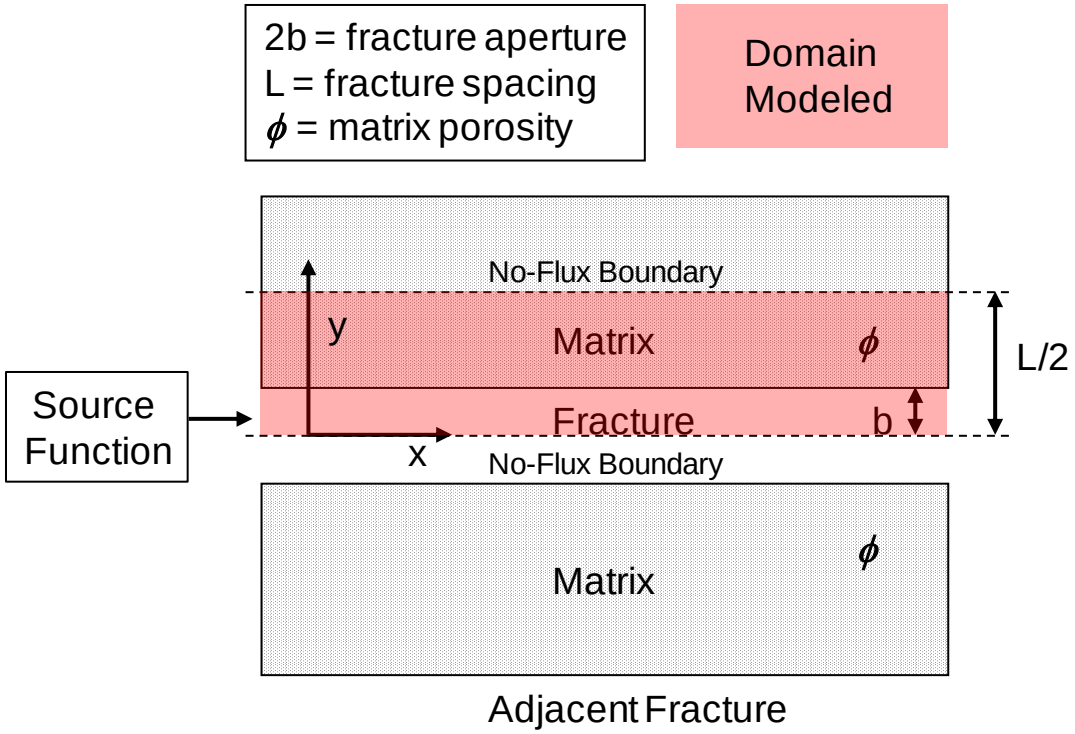

Figure 6. System geometry and boundary conditions assumed in the numerical model (also applies to the RELAP model).

The reaction processes accounted for by equations 1-12 are depicted in Figure 7 (including diffusion between the fractures and matrix). Solutes can adsorb to and desorb from two different sorption sites that are assumed to present on (1) fracture surfaces, (2) matrix surfaces, (3) mobile colloid surfaces, and (4) immobile colloid surfaces. One of the adsorption sites on each surface can be specified as being irreversible by simply specifying a desorption rate constant of zero for that site. Colloids can attach either reversibly or irreversibly to fracture surfaces, but they are not allowed to diffuse into the matrix. When the colloids attach or detach, they carry any adsorbed solutes with them, although the solutes can still independently adsorb or desorb from the colloids after the colloid transition. Additionally, colloid generation from fracture surfaces is allowed. The model ensures that a background colloid concentration given by P_{col}/k_{fci} is always maintained in the system, satisfying the steady-state condition that the colloid production rate must be balanced by an irreversible filtration rate (if this were not true either all colloids would disappear from the system or the system would plug with colloids). Each arrowhead in Figure 7 has a reaction rate that can be specified by the user (or a diffusion coefficient in the case of diffusion into/from the matrix).

The red-outlined boxes in Figure 7 were the only ones that were actually used to model the colloid and solute data from tracer test 12-02. Specifically, only a single type of sorption site was assumed to be present on each of the surfaces present in the system (although the fracture, matrix, and colloid sites were allowed to have different adsorption and desorption rates), and irreversible colloid filtration was ignored (meaning that colloid production from the fracture surfaces was also ignored). It was found that reasonable fits to the tracer data could be obtained without the black-outlined boxes, and it was considered desirable to not complicate the model

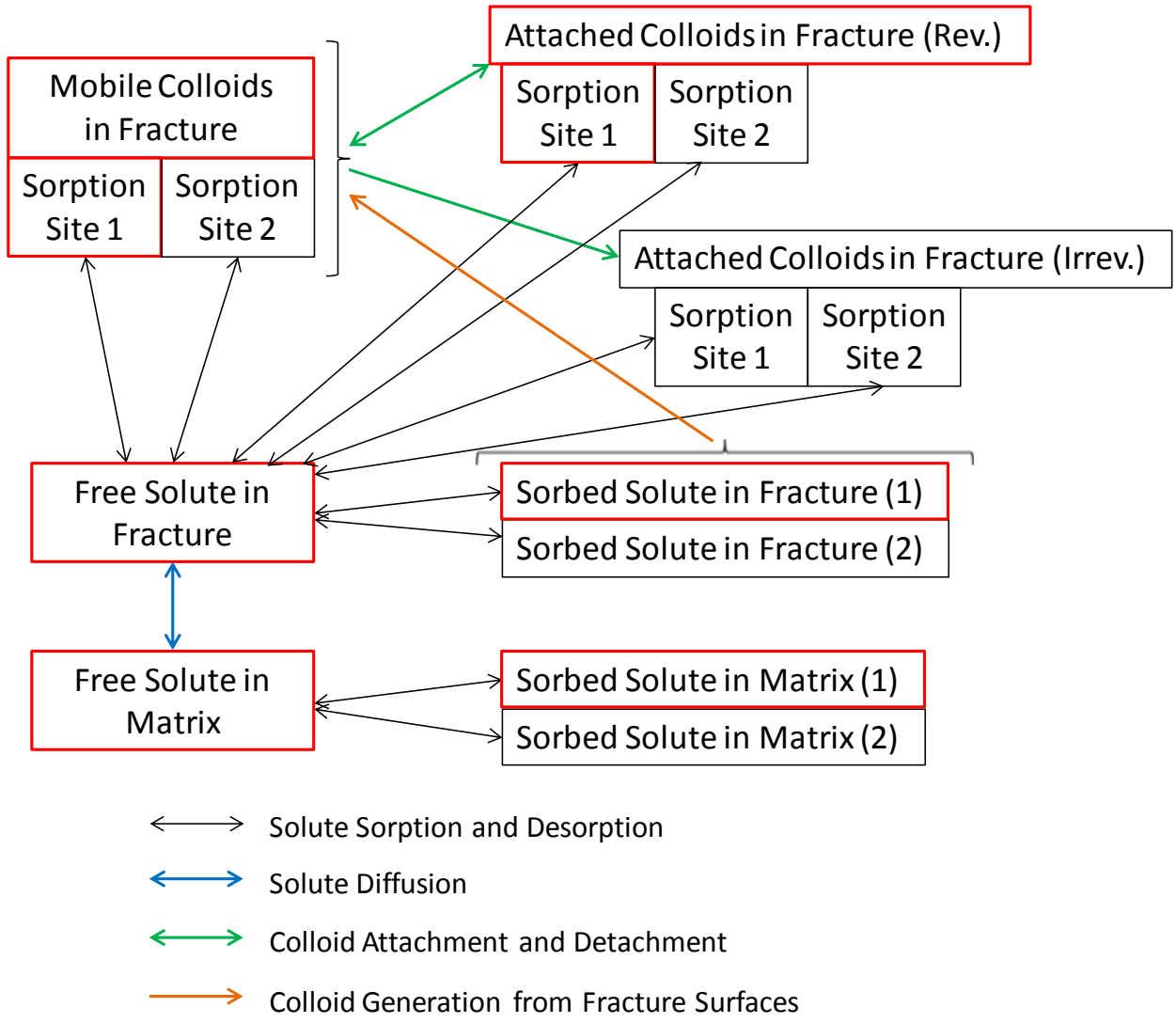

Figure 7. Reaction processes accounted for by equations 1-12 and implemented in the numerical transport model. Note that the red-outlined boxes were the only boxes actually used in the interpretation of tracer test 12-02.

with additional processes and parameters that did not significantly improve the fits; although it is recognized that adding more parameters will always result in a somewhat better fit.

Additional features of the numerical model that may be useful for tracer test interpretations include:

- The fraction of solute adsorbed onto colloids in the injection cocktail can be specified for each of the two sorption sites on the colloids.
- The colloid production rate (from fracture surfaces) can be specified to change during the test. This feature is provided so that any known transients in natural colloid concentrations (perhaps as a result of flow rate changes or flow interruptions) can be

simulated. Tests can also be simulated with only natural colloids present in the system and no colloids included in the injection cocktail. In this case, the transport of solutes can still be facilitated by the natural colloids present in the system.

- The source function can be specified as either a finite-duration pulse (i.e., a top-hat function) or as an exponentially-decaying function that has a decay constant equal to a specified injection flow rate divided by an injection circuit volume. In the latter case, the flow rate can be specified to change as many times as the user wants (but the injection circuit volume is fixed).
- Dilution resulting from differences between injection and extraction flow rates is automatically accounted for (note that the extraction flow rate is assumed to be constant). However, when the injection flow rate changes during a test, the dilution factor is not correspondingly changed because a rapid change in the injection flow rate would result in an unrealistic discontinuity in the extraction breakthrough curve. Rather, the initial dilution factor is retained throughout the simulated test.
- Different Peclet numbers can be specified for the solutes and colloids in the same simulation.

Interpretive Results

Figure 8 shows the numerical model fits to the AGA and colloid breakthrough curves from tracer test 12-02. The colloid breakthrough curve was matched assuming slow, reversible filtration in the fractures and a somewhat smaller Peclet number (larger dispersivity) than the solutes to account for the slightly earlier arrival of the colloids relative to the AGA. The AGA breakthrough curve was not actually fitted but was reproduced using the parameters from the RELAP semi-analytical model fitting exercise as a way of verifying that the numerical model was functioning properly. However, unlike in the RELAP exercise, a small amount of matrix diffusion was assumed for the AGA in the numerical model to be consistent with the matrix diffusion assumed for the other solutes. It was found to be necessary to invoke some matrix diffusion and adsorption in the matrix to explain the breakthrough curve of ^{22}Na. In all numerical model simulations, a 2-mm fracture aperture with an internal porosity of 0.5 was assumed and a 1-cm-thick "rim zone" of porosity 0.05 was assumed along the fracture walls to represent the altered shear zone. Also, all the solutes with the exception of AGA were assumed to have a matrix diffusion coefficient of 1×10^{-6} cm^2/sec (the AGA was assumed to have a diffusion coefficient of 2×10^{-7} cm^2/sec because of its larger molecular size). The sensitivity of the model results to these parameter values was not evaluated in this preliminary exercise.

Figures 9 through 13 show the model fits to each of the radionuclide breakthrough curves for which data were available. In Figures 10-13, the model-simulated solute and colloid contributions to the overall predicted radionuclide breakthrough curves are also shown. Figure 9 shows only a single curve because ^{22}Na was assumed to transport only as a solute because of the observation that it did not partition at all to the colloids in the injection cocktail (Schäfer, presentation to CFM working group, June 2012). For all other radionuclides except for ^{243}Am, the majority of the breakthrough was predicted to be associated with colloids. The results for ^{243}Am are considered suspect because of the known strong partitioning of Am to the bentonite colloids (Huber et al., 2011) and the fact that any Am desorbed from colloids would be expected to adsorb strongly to immobile surfaces in the system. However, the relatively late arrival and

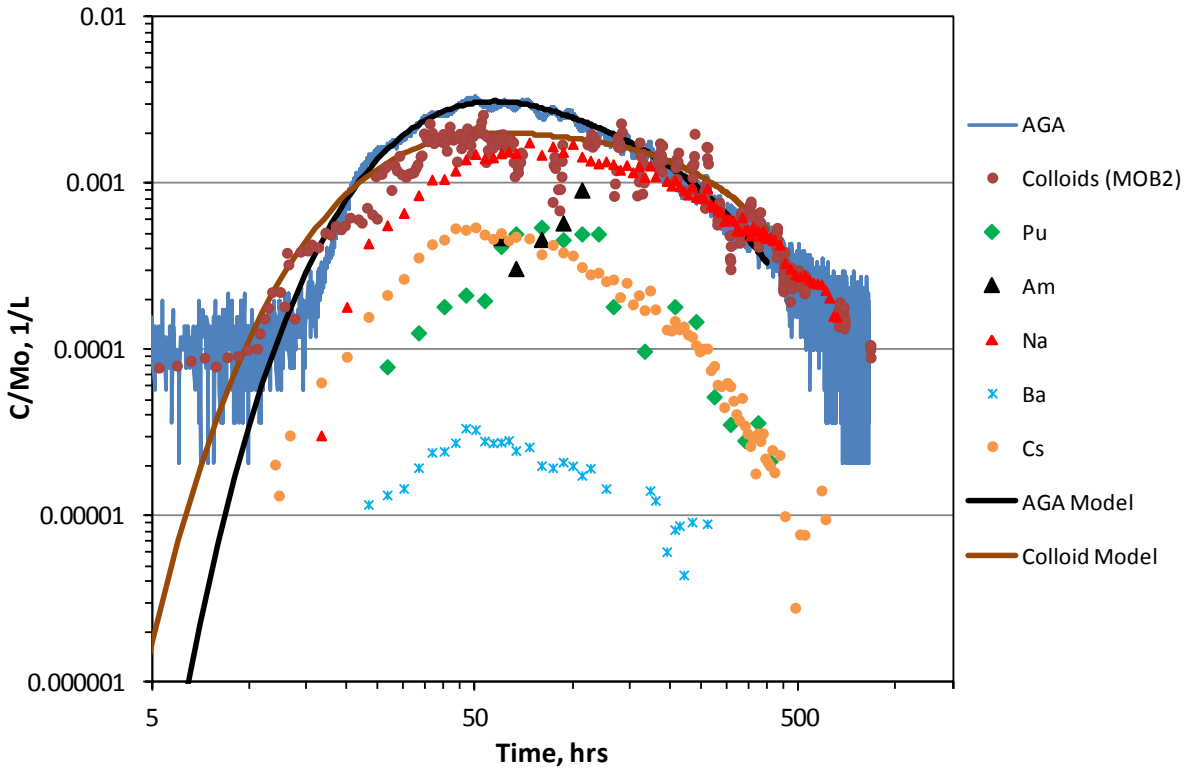

Figure 8. Numerical model matches to the AGA and colloid breakthrough curves in CFM test 12-02.

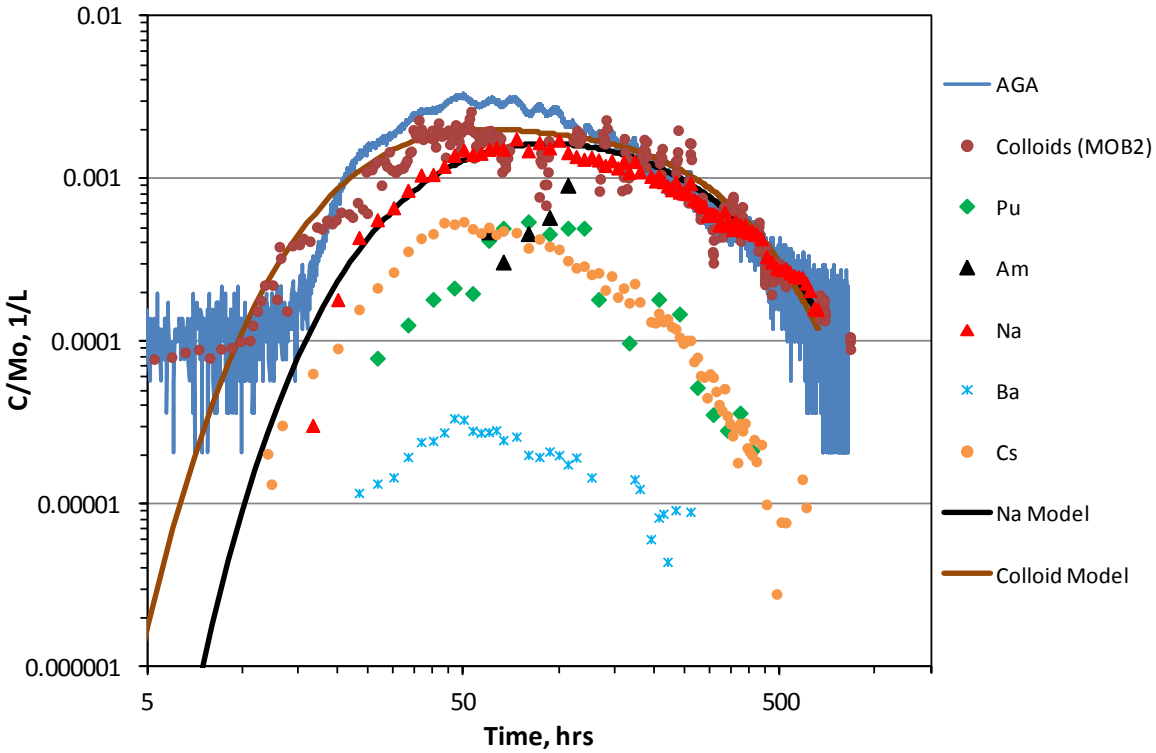

Figure 9. Numerical model matches to the ^{22}Na and colloid breakthrough curves.

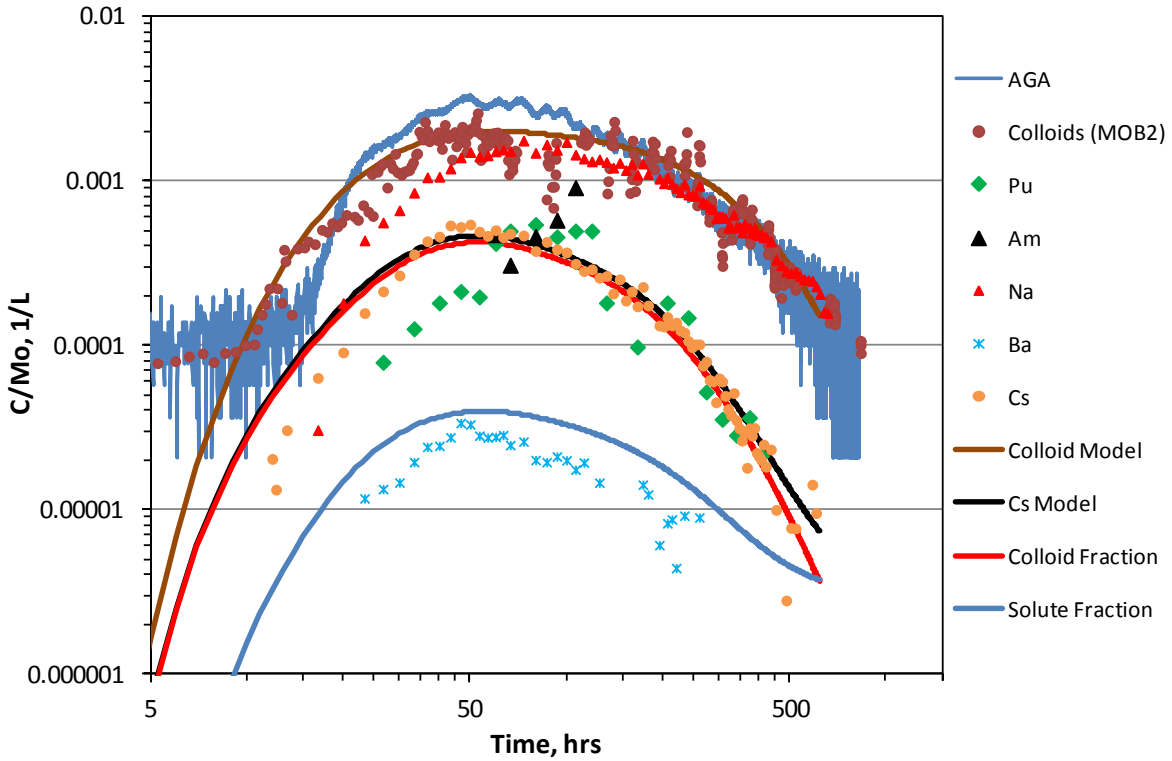

Figure 10. Numerical model matches to the ^{137}Cs and colloid breakthrough curves.

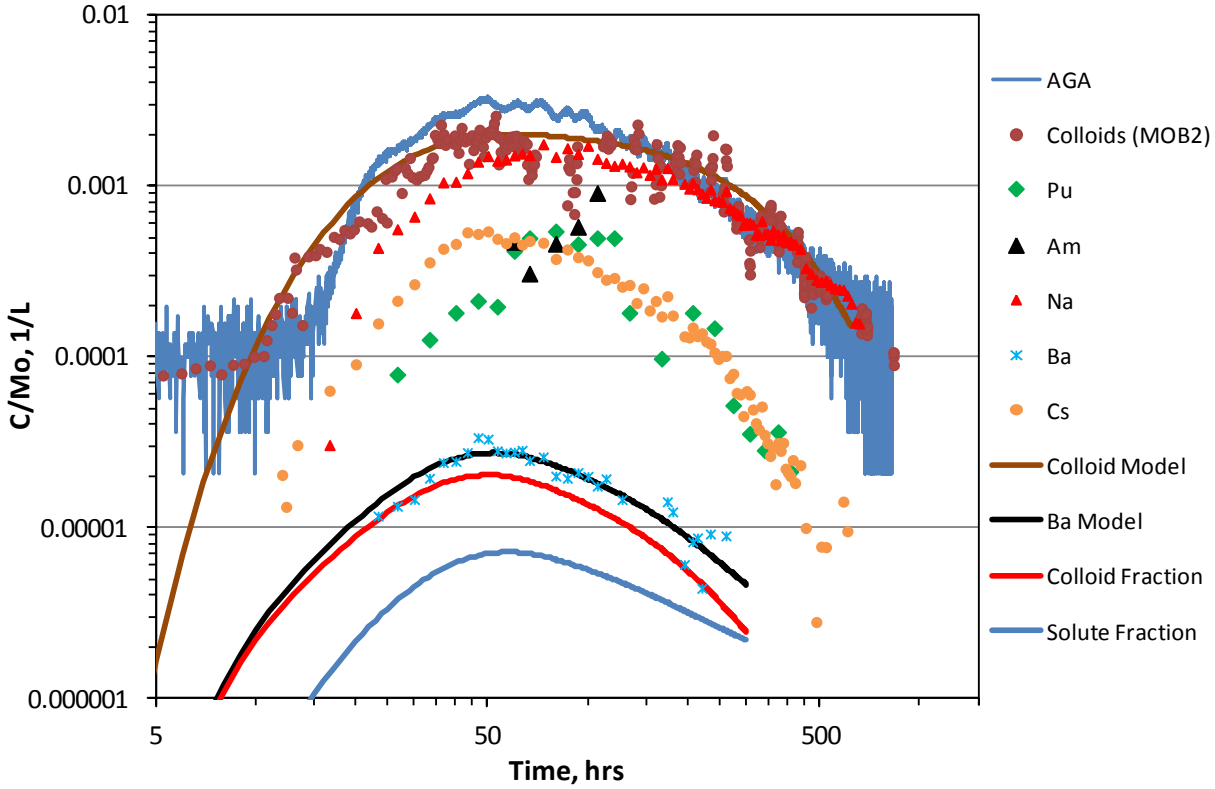

Figure 11. Numerical model matches to the ^{133}Ba and colloid breakthrough curves.

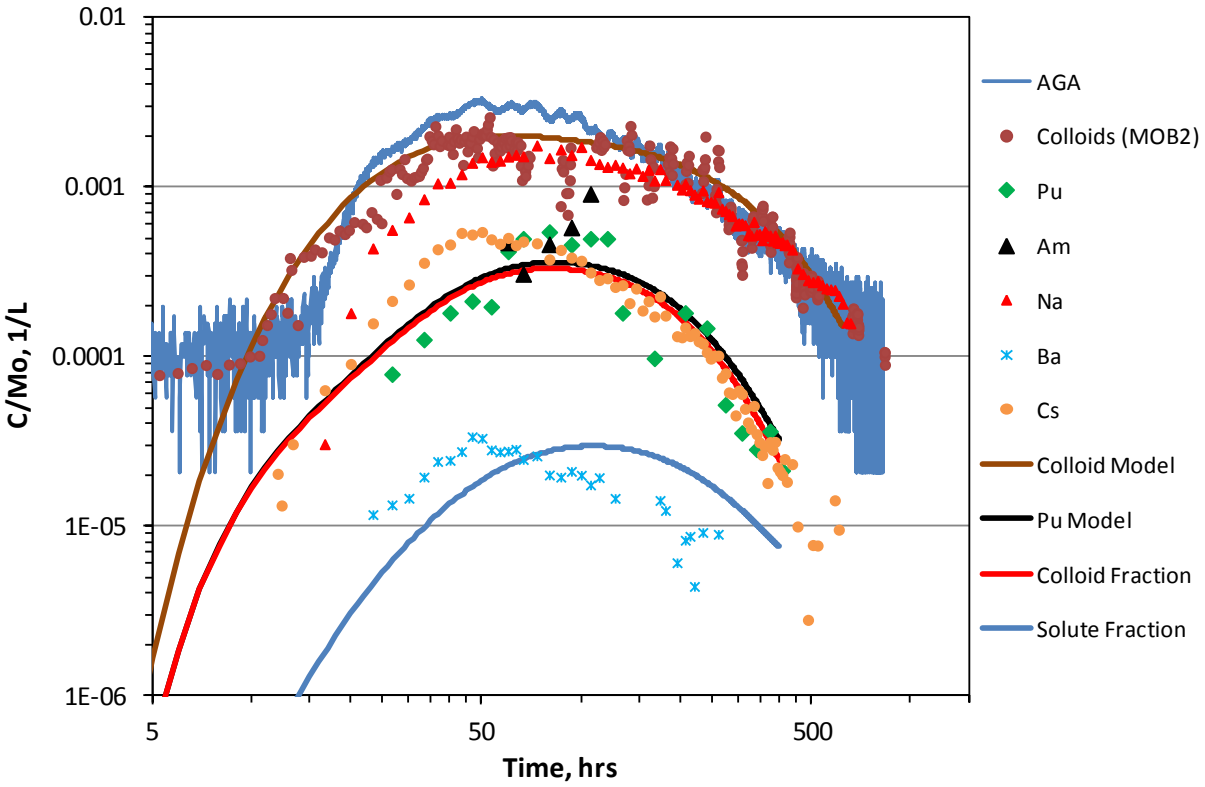

Figure 12. Numerical model matches to the ^{242}Pu and colloid breakthrough curves.

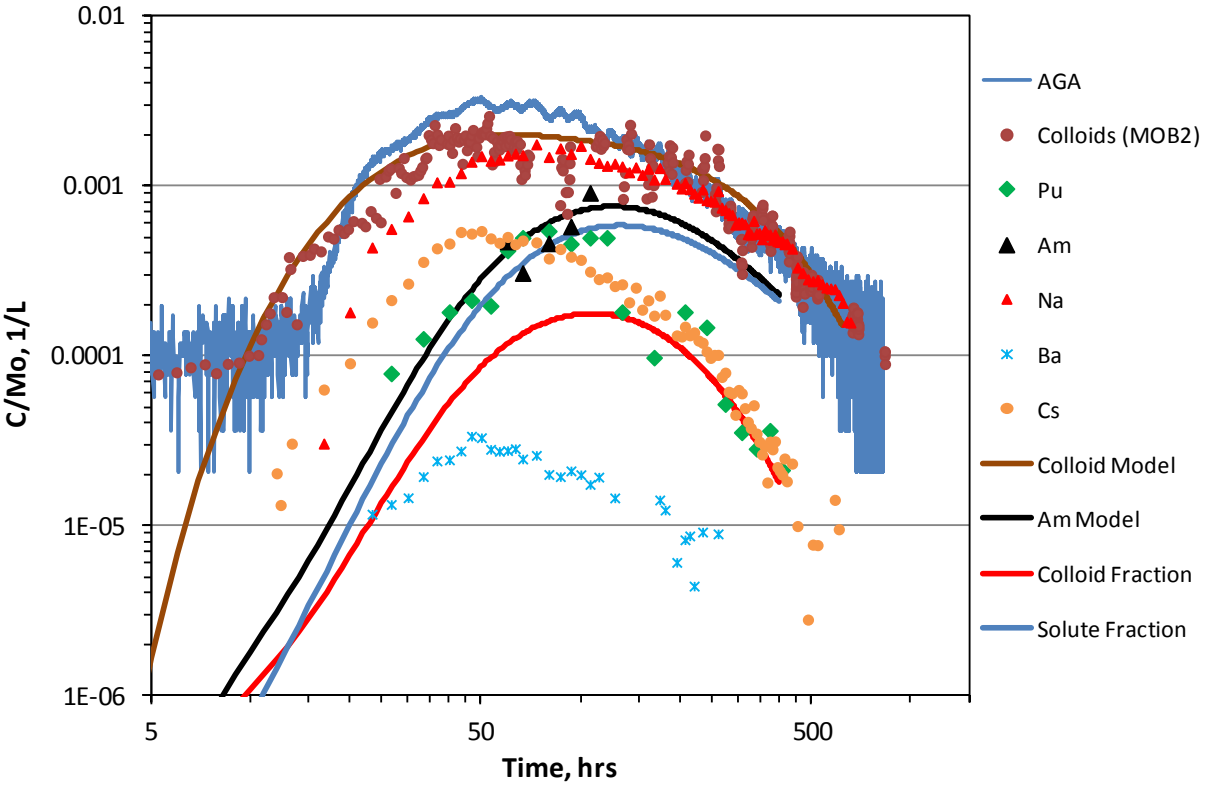

Figure 13. Numerical model matches to the ^{243}Am and colloid breakthrough curves.

high normalized concentrations of the ^{243}Am deduced from the very few data points available for this radionuclide could not be reconciled with a predominantly colloid-associated breakthrough. Rather, relatively rapid desorption of the ^{243}Am from the colloids had to be assumed along with weak adsorption/retardation of the soluble ^{243}Am in the fractures and matrix to achieve a reasonable match to the data. It is unknown whether the small number of ^{243}Am data points accurately represents the ^{243}Am transport behavior, and it is recommended that the results of Fig. 13 be considered very preliminary until more data become available.

The reaction rate constants associated with each of the model fits in Figures 8 through 13 are listed in Table 2. All the solutes were assumed to have the same mean residence time, Peclet number, and mass fraction participation as the AGA, so only reaction rate constants were adjusted to match the radionuclide breakthrough curves. It is emphasized that these parameters were not estimated by a rigorous quantitative parameter estimation technique but rather they were obtained by manual adjustment of the parameter values until a reasonable match to the data was visually achieved. The colloid breakthrough curve was matched by adjusting the colloid Peclet number and the filtration and detachment rate constants while assuming the same mean residence time and mass fraction participation as the AGA.

Table 2. Reaction rate constants used to obtain the model curves of Figures 8 through 13. Note that the sensitivity of the model results to the parameter values was not evaluated. Also, the uniqueness/nonuniqueness and uncertainty of the parameter values were not evaluated.

	-----Fracture Surfaces----		-----Matrix Surfaces-----		-----Colloid Surfaces------	
Tracer	k_{fa}**, ml/g-hr**	k_{ra}**, 1/hr**	k_{fam}**, ml/g-hr**	k_{ram}**, 1/hr**	k_{1f}**, ml/g-hr**	k_{1r}**, 1/hr**
^{22}Na	0	0	6.85	10	0	0
^{137}Cs	3	1	5	0.001	30,000	0.2
^{133}Ba	3	1	5	0.0025	10,000	0.4
^{242}Pu	40	3	5	1	45,000	0.25
^{243}Am	4	3	0.02	0.001	4500	0.65
	k_{fc}**, 1/hr**	k_{rc}**, 1/hr**	k_{fci}**, 1/hr**			
Colloids	0.02	0.0125	-0-			

Note that the very small matrix desorption rate constants for the ^{137}Cs and ^{133}Ba ensure that the matrix acts as a sink for these two radionuclides once they desorb from the colloids.

Discussion

The results presented in the previous section suggest that the ^{137}Cs, ^{133}Ba, and ^{242}Pu breakthroughs in test 12-02 were all highly associated with colloids. However, the fact that the recoveries of these radionuclides were significantly lower than that of the colloids also suggests that there was significant desorption of each from the colloids during the tracer test. This desorption was apparently faster than the desorption rate of the homologues Th, Hf, Eu, and Tb from FEBEX bentonite colloids in previous colloid-homologue tracer tests 10-01 and 10-03 (Kersting et al., 2012). Laboratory desorption data for Cs and Ba from the colloids were not available for comparison with the field test results, but Pu and Am desorption data were available from the work of Huber et al. (2011). Huber et al. (2011) conducted desorption experiments in

which Pu and Am were initially adsorbed onto FEBEX bentonite colloids that were dispersed in Grimsel groundwater and were then placed in contact with "fracture fill material" obtained from the MI shear zone at Grimsel. A time series of samples from these experiments were analyzed for Pu and Am in the bulk solution phase and in an ultra-centrifuged aliquot of each sample, and the results were used to estimate desorption rates from the colloids in the presence of the fracture fill material. Interestingly, faster desorption rates were observed in experiments with lower starting concentrations of the Pu and Am adsorbed to the colloids, but even these faster rates would have resulted in much greater colloid-facilitated transport of the Pu and Am than was observed in tracer test 12-02.

Figure 14 shows the breakthrough curves of Pu and Am predicted for test 12-02 using the highest desorption rate constants deduced from the experiments of Huber et al. (2011), with all other parameters kept the same as in Table 2. It is obvious that the breakthrough curves of Pu and Am are both significantly overpredicted using the laboratory-derived parameters. Clearly, it seems that processes occurred in the field experiment that were not well represented in the laboratory experiments, although further analysis and evaluation should await finalization of the Pu and Am data. As noted in the previous section, the Am data should especially be verified and ideally supplemented with additional data points, as the small number of data points currently available suggests very little colloid-facilitated transport of the Am, which not only conflicts with the laboratory results of Huber et al. (2011) but also with previous observations of colloid-facilitated Am transport in tracer test #32 of the Colloid and Radionculide Retardation (CRR) project at Grimsel in which Am transport was highly associated with bentonite colloids (Möri et al., 2004). This CRR experiment was conducted in the MI shear zone in a dipole between two boreholes, although it had a much shorter residence time in the shear zone than test 12-02. Interestingly, Am and Pu also transported quite efficiently (essentially conservative transport of a significant fraction of the injection mass) in CRR tracer test #31 in which no bentonite colloids were injected. It is suspected that much of this transport was associated with natural colloids present in the system or perhaps colloids inadvertently present in the injection cocktail (Möri et al. 2004).

The observed breakthrough curve of the ^{22}Na in test 12-02 is consistent with the transport of a weakly- and reversibly-sorbing solute that adsorbs primarily in the matrix after diffusion out of fractures. The lower and slightly delayed peak concentration of the ^{22}Na relative to the AGA and the suggestion of a crossing of the tails of the two breakthrough curves at late times are all hallmarks of dual-porosity transport of a weakly-sorbing solute. The ratio of the model-derived matrix adsorption rate constant to the desorption rate constant for ^{22}Na in Table 2 suggests a matrix partition coefficient, or K_d value, of 0.68 ml/g, which is indeed a relatively small value for a partition coefficient.

In contrast to ^{22}Na, the breakthrough curves of the ^{137}Cs, and ^{133}Ba are not consistent with dual-porosity transport of a solute. This inconsistency is perhaps best illustrated by examining breakthrough curves from some of the Tracer Retention Understanding Experiments (TRUE) tracer tests conducted in a fractured granite at the Aspö field site in Sweden, where it was concluded that several cationic radionuclides exhibited classic dual-porosity behavior with adsorption in a "rim zone" along fracture walls (Andersson et al., 2002). Figure 15 shows the breakthrough curves of several radionuclides in TRUE tracer tests in which no colloids were

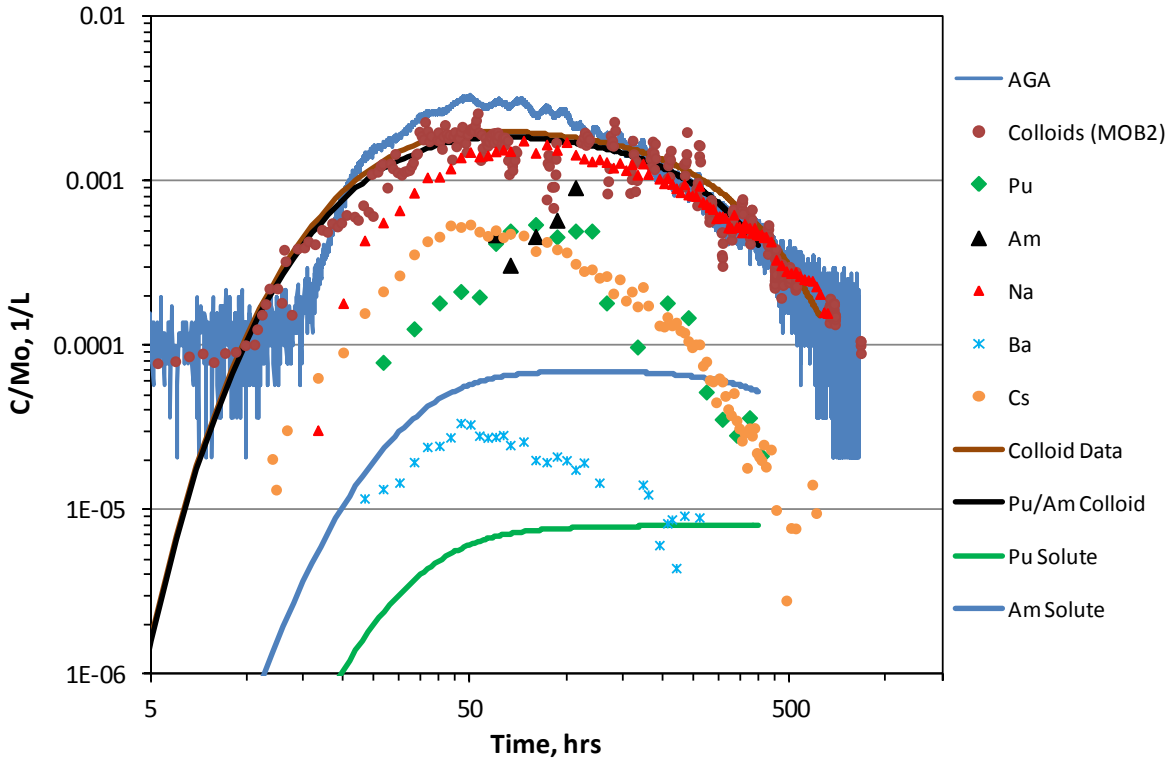

Figure 14. Predicted ^{242}Pu and ^{243}Am breakthrough curves using the colloid desorption rate constants from the ternary desorption experiments of Huber et al. (2011) (k_{1r} = 0.0085 hr^{-1} for Pu and 0.009 hr^{-1} for Am). All other reaction rate constants are the same as in Table 2. The predicted breakthrough curves are dominated by colloid-facilitated radionuclide transport. The Pu-colloid and Am-colloid model curves are essentially indistinguishable.

intentionally introduced in the injection cocktails. Here it is evident that while the ^{24}Na breakthrough curve is qualitatively similar to the ^{22}Na breakthrough curve in test 12-02, the breakthrough curves of ^{134}Cs and ^{131}Ba are both significantly different than the curves of the Cs and Ba isotopes in test 12-02. The breakthrough curves of the isotopes in test 12-02 have earlier first and peak arrivals and do not exhibit crossovers in the tails of the breakthrough curves as in the TRUE tests. These features are all consistent with colloid-facilitated transport behavior in test 12-02. Although the mineralogy and water chemistry in the two systems are different, the fact that the Ba has an earlier and higher peak than Cs in the TRUE tests but a lower peak than Cs in test 12-02 is also strongly suggestive of colloid-facilitated transport of these radionuclides in test 12-02. Cs is generally expected to be a stronger cation exchanger than Ba in most mineralogic systems, so the behavior in the TRUE tests would also be expected at Grimsel in the absence of colloid-facilitated transport. However, in the presence of the bentonite colloids, the stronger cation exchanging behavior of the Cs caused it to be more strongly adsorbed to the bentonite colloids than the Ba and thus to be transported more efficiently through the flow system than the Ba.

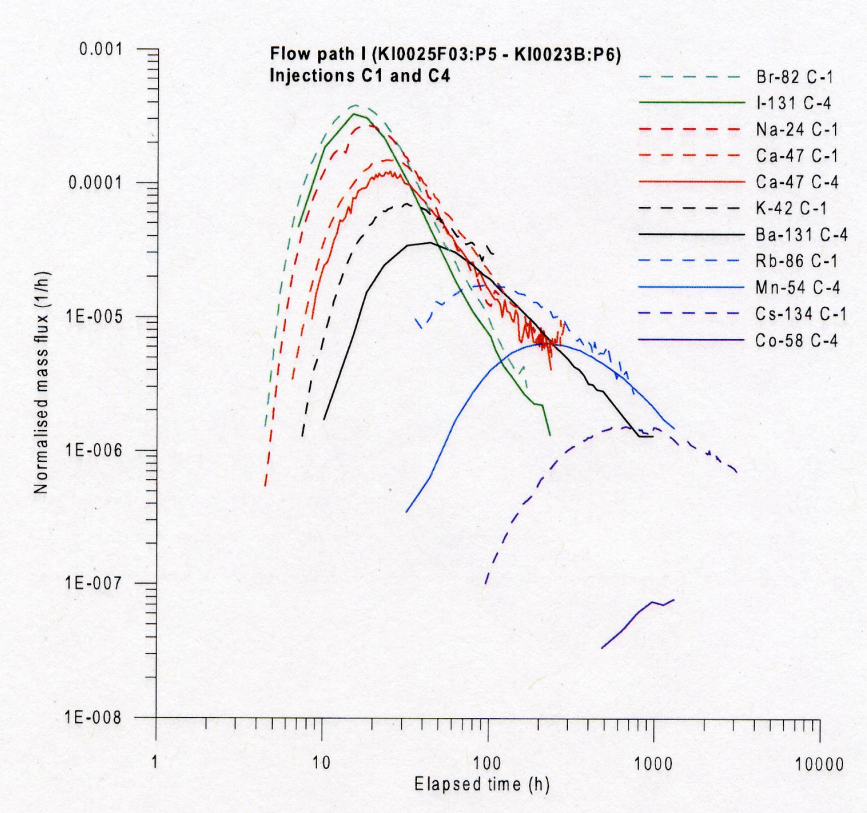

Figure 15. Breakthrough curves of several cations relative to conservative tracers (Br and I) in fractured granite at the Aspö site in Sweden (Taken from Andersson et al., 2002, Fig. 6-11).

Interestingly, in CRR test #32, ^{137}Cs also exhibited colloid-faciliated transport behavior, although in contrast to test 12-02, the colloid facilitation was much less than Pu (Möri et al., 2004, Figure 4.19). Also, in CRR test #32 there was a second, much later, ^{137}Cs peak observed that can probably be attributed to solute transport of the ^{137}Cs that was not associated with the colloids. A second ^{137}Cs peak in test 12-02 was not evident, presumably either because too much of the ^{137}Cs was adsorbed to the colloids or because the test was not conducted long enough to see a second peak. Ba was not used in the CRR experiments, so no comparison could be made to the ^{133}Ba transport behavior observed in test 12-02. However, based on the TRUE test results, it would not have been surprising to see a second and higher peak of ^{133}Ba if the test had been conducted longer.

Conclusions

CFM tracer test 12-02 provided a successful "shakedown" for the eventual radionuclide-doped bentonite emplacement experiment that will be conducted in the same test configuration at the Grimsel Test Site, probably starting in 2013. It is extremely valuable to obtain breakthrough curves under the conditions of test 12-02 for the colloids and for several of the same elements that will be used in the bentonite emplacement experiment so that quantitative inferences can be drawn about the processes occurring in the emplacement experiment by comparing breakthrough curves with those of test 12-02. Lessons learned with respect to some of the analytical challenges (very low detection limits needed for several of the elements) are also very valuable.

The bentonite colloid breakthrough curve in CFM test 12-02 was consistent with weak and reversible filtration of the colloids, although the dispersion of the colloids in the fracture(s) was deduced to be slightly greater than that of the solutes. This behavior is generally consistent with the colloid transport behavior observed in previous CFM colloid-homologue tracer tests in the same test configuration (10-01 and 10-03), although each test had its own signature features (10-01 had a later colloid first arrival than the conservative solute, 10-03 had nearly a simultaneous colloid and conservative solute first arrival, and 12-02 had an earlier colloid arrival).

The transport behavior of the ^{22}Na in CFM tracer test 12-02 was consistent with dual-porosity transport of a weakly and reversibly sorbing solute that sorbs primarily in the matrix after diffusing out of fractures. Colloid-facilitated transport of the ^{22}Na was not evident, consistent with the fact that virtually none of the ^{22}Na in the injection cocktail was adsorbed to colloids. The transport behavior of the ^{137}Cs and ^{133}Ba in test 12-02 were consistent with moderately strong and much weaker colloid-facilitated transport, respectively, with very little of the recovered mass/activity of these two radionuclides eluting as solutes. The ^{242}Pu transport behavior in test 12-02 was also consistent with colloid-facilitated transport, although the apparent rate of Pu desorption from the bentonite colloids was much faster than in the ternary system laboratory experiments of Huber et al. (2011). The transport of ^{243}Am in test 12-02 was deduced to be mostly as a solute, with relatively rapid desorption of the ^{243}Am from the colloids and only weak retardation of the resulting soluble ^{243}Am in the fractures and matrix. This deduced behavior is not consistent with either laboratory experiments or previous CRR experiments conducted in the MI shear zone at Grimsel, so this conclusion should be considered very preliminary until either more ^{243}Am data are generated or the small number of existing data points are verified and/or refined.

Besides updating interpretations of the tracer test as more data become available or as data are refined, future modeling efforts should focus on evaluating the sensitivity of the model results to the reaction rate constants used in the numerical model. Also, the reaction rate constants of Table 2 almost certainly do not provide uniquely good matches to the radionuclide breakthrough curves, so the (non)uniqueness and uncertainty of these rate constants should be evaluated in future efforts.

References

Andersson, P., J. Byegard, and A. Winberg, 2002. Final Report of the TRUE Block Scale project. 2. Tracer tests in the block scale. *Technical Report TR-02-14*, Swedish Nuclear Fuel and Waste Management Co., Stockholm, Sweden.

Arnold, B. A., Reimus, P. W., and James, S. C., 2011. Flow and Transport in Saturated Media: FY2011 Status Report. Prepared for U.S. Department of Energy Used Fuel Disposition Campaign, *FCRD-USED-2011-000311*, Sandia National Laboratories and Los Alamos National Laboratory.

Huber, F., Kunze, P, Geckeis, H., and Schäfer, T. 2011. Sorption reversibility kinetics in the ternary system radionuclide-bentonite colloids/nanoparticles-granite fracture filling material, *Appl. Geochem.*, 26, 2226-2237.

Kersting, A., Zavarin, M., Zhao, P., Dai, Z. Carroll, S., Wang, Y., Miller, A., James, S., Reimus, P., Zheng, L., Li, L., Rutqvist, J., Liu, H.-H., and Birkholzer, J. 2012. Radionuclide Interaction and Transport in Representative Geologic Media, Prepared for U.S. Department of Energy Used Fuel Disposition Campaign, *FCRD-UFD-2012-000154*, Sandia National Laboratories.

Möri, A. (Ed.). 2004. The CRR final project report series I: Description of the Field Phase – Methodologies and Raw Data. *Nagra Technical Report NTB 03-01*. Nagra, Wettingen, Switzerland.

Reimus, P. W., Pohll, G., Mihevc, T., Chapman, J., Papelis, L., Lyles, B., Kosinski, S., Niswonger, R., and Sanders, P., 2003. Testing and parameterizing a conceptual model for radionuclide transport in a fractured granite using multiple tracers in a forced-gradient test, *Water Resour. Res.*, **39**(12), p. 1350, doi:10.1029/2002WR001597.